

Article

Properties of Mechanically Alloyed W-Ti Materials with Dual Phase Particle Dispersion

František Lukáč^{1,*}, Monika Vilémová¹, Barbara Nevrlá¹, Jakub Klečka¹, Tomáš Chráska¹ and Orsolya Molnárová²

¹ Institute of Plasma Physics, Czech Academy of Science, Za Slovankou 3, 18200 Prague, Czech Republic; vilemova@ipp.cas.cz (M.V.); nevrta@ipp.cas.cz (B.N.); klecka@ipp.cas.cz (J.K.); tchraska@ipp.cas.cz (T.C.)

² Mathematics and Physics Faculty, Charles University, Ke Karlovu 3, 12116 Prague, Czech Republic; mopersze@gmail.com

* Correspondence: lukac@ipp.cas.cz; Tel.: +420-266053077

Academic Editor: Chun-Liang Chen

Received: 31 October 2016; Accepted: 20 December 2016; Published: 26 December 2016

Abstract: W alloys are currently widely studied materials for their potential application in future fusion reactors. In the presented study, we report on the preparation and properties of mechanically alloyed W-Ti powders compacted by pulsed electric current sintering. Four different powder compositions of W-(3%–7%)Ti with Hf or HfC were prepared. The alloys' structure contains only high-melting-point phases, namely the W-Ti matrix, complex carbide (Ti,W,Hf)C and HfO₂ particle dispersion; Ti in the form of a separate phase is not present. The bending strength of the alloys depends on the amount of Ti added. The addition of 3 wt. % Ti led to an increase whereas 7 wt. % Ti led to a major decrease in strength when compared to unalloyed tungsten sintered at similar conditions. The addition of Ti significantly lowered the room-temperature thermal conductivity of all prepared materials. However, unlike pure tungsten, the conductivity of the prepared alloys increased with the temperature. Thus, the thermal conductivity of the alloys at 1300 °C approached the value of the unalloyed tungsten.

Keywords: tungsten-titanium alloys; mechanical alloying; particle dispersion; pulsed electric current sintering; thermal conductivity; bending strength

1. Introduction

With the progress of nuclear fusion research, the need for new, advanced materials is becoming more urgent. For the International Thermonuclear Experimental Reactor (ITER), the choice of materials has been made. Thus, the area of the ITER's first wall will be covered by armor produced from beryllium and the exhaust components will be covered by tungsten. However, materials for the next step of reactors will have to satisfy strict requirements for the lifetime and safety levels. Thus, nontoxic, highly durable and functional materials would be the prime choice for tokamak such as DEMO tokamak.

Until recently, pure tungsten was considered the most suitable plasma-facing material for the future reactor's first wall. Its superiority over other materials was granted by the following group of properties: high resistance to sputtering, high melting point, good thermal conductivity, low thermal expansion and low tritium retention. Nevertheless, tungsten also has certain disadvantages, with thermally induced grain growth (depending on its thermomechanical history, starting at temperatures as low as 1000 °C) among the most serious. Thus, in the conditions of fusion plasma and plasma disruptions, excessive grain growth leads to the degradation of mechanical properties, which subsequently causes premature failure of the plasma-facing component during heat cycling. A further problem arises during exposure of the tungsten to the irradiated particles, such as those of

helium and deuterium present in the fusion plasma. The particles penetrate into the material bulk and under specific conditions, such as high particle fluencies, the crystalline lattice becomes supersaturated which leads to blister or helium fuzz formation [1] and, therefore, the further degradation of the mechanical properties. Another concern of tungsten's behavior is related to the formation of tungsten oxides in the presence of oxygen. Tungsten trioxide represents a serious risk in the case of reactor accidents under which oxygen or oxygen-containing compounds (such as coolant water) enter the reactor chamber. The formation of volatile tungsten trioxide could lead to radiation escaping into the surrounding environment. Thus, efforts to develop a smart tungsten material that can suppress thermal and radiation degradation as well as the formation of volatile oxides have emerged recently.

Most recent attempts to improve tungsten properties have been conducted through the modification of tungsten's microstructure and the addition of minor alloying elements. Many of the developed materials show promising results. For example, some studies point out that ultrafine-grained tungsten not only has better mechanical properties but is also significantly more resistant to irradiation from ions [2]. In order to stabilize the grain size at higher temperatures, tungsten with a particle dispersion has been developed. In the case of tungsten, usually small amounts of oxides, e.g., Y_2O_3 , La_2O_3 (ODS—oxide dispersion strengthening), or carbides of transition metals, e.g., TiC (CDS, carbide dispersion strengthening), are added [3,4]. The suppression of the formation of volatile tungsten oxide has been suggested by the formation of tungsten self-passivating alloys [5] consisting of W with the addition of Cr and Ti or Si. In the oxidation atmosphere, complex Cr-W oxide layers are formed, encapsulating the tungsten oxides at the surface of the armor. However, the effect of the various alloying elements is still being studied.

Since the melting temperature of tungsten is the highest among the chemical elements, the powder metallurgy accompanied by mechanical alloying is the obvious choice of alloying method. The spark plasma sintering method provides the exceptional advantage of fast heating/cooling rates when compared to conventional sintering methods. Therefore, a high sintering temperature is achieved simultaneously with the suppression of unwanted grain growth. In the present study, we attempted to prepare W-Ti alloys with the addition of HfC or Hf by means of mechanical alloying. According to our experience, HfC has a tendency to oxidize either during mechanical alloying or during sintering to form HfO_2 . In this way, the mitigation of Ti oxidation was approached. The alloys were analyzed for their phase composition during each individual step of the preparation. Thus, the alloying process can be better understood and used for further tailoring of the alloys. The phases were correlated with the microstructural information. Basic mechanical properties of the prepared alloys were analyzed and the effect of the addition of Ti was discussed. The effect of the alloying elements on room- and high-temperature thermal conductivity was studied as it remains overlooked in the majority of published studies due to the low amounts of alloying elements.

2. Materials and Methods

The powder batches of composition W-3 wt. % Ti-2 wt. % HfC, W-7 wt. % Ti-2 wt. % HfC, W-3 wt. % Ti-2 wt. % Hf and W-7 wt. % Ti-2 wt. % Hf (see Table 1) were prepared in a planetary ball mill Pulverisette 5 (Fritsch, Germany). The starting powders were W (99.9% purity, 1.2 μm average powder size), Ti (99.4% purity, 5 μm average powder diameter size), Hf (bimodal powder diameter size distribution, 15 μm and 45 μm) and HfC (bimodal powder diameter size distribution, 5 μm and 20 μm). For the ball milling process, the powders were loaded in tungsten carbide bowls with tungsten carbide grinding balls in the ball to powder ratio (BPR) 11:1. High purity argon was used as protective atmosphere in order to prevent oxidation during the milling process. The summary of the milling parameters can be found in Table 1. The powders were consolidated by pulsed electric current sintering machine SPS 10-4 (Thermal Technology, Santa Rosa, CA, USA) under similar sintering conditions, i.e., sintering temperature 1750 $^{\circ}\text{C}$, pressure of 70 MPa, vacuum of 10 Pa and sintering time of 3 min. Sintering was performed in graphite molds and graphite foils or graphite foils covered by hexagonal boron nitride (BN). All milling and sintering parameters are summarized in Table 1.

Table 1. Summary of the materials and production conditions.

Sample Designation *	Starting Powders (Average Size, μm)	Ball Milling Conditions	Sintering Conditions
W-3Ti-2HfC	W (1.2), Ti (5), HfC (bimodal 5 and 20)	11:1 (BPR), 30 min mixing at 80 RPM 270 rpm (milling speed), 40 h (milling time), Argon atmosphere, WC-Co milling bowls and balls.	100 °C/min (Heating speed), 1750 °C sintering temperature, 3 min hold time at 1750 °C, powder surrounded by a graphite foil, vacuum, 120 ms/30 ms on/off pulses at started at sintering temperature.
W-7Ti-2HfC			
W-3Ti-2Hf	W (1.2), Ti (5), Hf (bimodal 15 and 45)		Identical to the above except that powder was surrounded by a graphite foil covered by BN (boron nitride) layer.
W-7Ti-2Hf			
W	W (1.2)	no ball milling	Identical to the above (W + Ti + Hf case)

* Numbers refers to weight percentage.

Phase compositions and lattice parameters were determined from X-ray diffraction (XRD) patterns obtained at room temperature by $\text{CuK}\alpha$ (divergent beam was used for mechanically alloyed powders and parallel beam of 1 mm diameter in the middle of the cross section cut was used for sintered samples) and 1D LynxEye detector (Bruker, Karlsruhe, Germany) ($\text{Ni } \beta$ filter in front of the detector) mounted on Bruker D8 Discover (Bruker, Karlsruhe, Germany) and subsequent Rietveld refinement [6] was performed in TOPAS 5 (Bruker, Karlsruhe, Germany) [7].

The flexure strength was measured using universal tensile test machine Instron 1362 (Instron, High Wycombe, UK) with support diameter of 5 mm, support span of 14.55 mm and loading rate of 0.2 mm/min.

The hardness was evaluated on a universal hardness tester Nexus 4504 (Innovatest, Maastricht, The Netherlands) using Vickers indenter, load equivalent to 1 kg and dwell time of 10 s.

The microstructure was evaluated on polished cross-sections using SEM EVO MA 15 (Carl Zeiss SMT, Oberkochen, Germany) in backscattered mode and equipped with EDS detector XFlash[®] 5010 (Bruker, Karlsruhe, Germany).

The thermal diffusivity (α) and specific heat capacity (C_p) of the samples were measured by a laser-flash method on an LFA 1000 apparatus (Linseis, Selb, Germany) in vacuum at RT, 100, 300, 500, 700, 900, 1100 and 1300 °C. The thermal conductivity (λ) was calculated utilizing the relationship $\lambda = \rho\alpha C_p$, where ρ is material density. The samples were cut into 10 mm \times 10 mm size and thickness was approximately 2 mm. Data were averaged from at least four measurements at each temperature.

3. Results

3.1. Microstructural and Phase Analysis

Table 2 shows the results of the Rietveld refinement of XRD diffractograms in the mechanically alloyed powders used in this study. The lattice parameters were significantly larger than the lattice parameter of pure tungsten at room temperature $a = 0.3165$ nm [8]. The dissolution of Ti in W continuously increased the lattice constant of the bcc phase β -(Ti,W) up to the lattice constant of the bcc Ti phase, which was close to 0.3283 nm [9]. Since no other phases of pure Ti or Hf were observed, one can conclude that the alloying elements Ti and Hf were introduced to the matrix of bcc W and formed a solid solution. Significant refinement of the crystallites' size was found in all milled powders after the high-energy milling, and microstrain values suggested that a substantial degree of deformation energy was stored in the powders.

Table 2. Results of Rietveld refinement fit for tungsten matrix phase in mechanically alloyed powders for 40 h. Fit errors of the last digit are given in parentheses.

Composition	Lattice Parameter a (nm)	Crystallite Size (nm)	Microstrain ϵ_0 (10^{-3})
W-3Ti-2HfC	0.317536 (8)	11.9 (1)	3.88 (3)
W-7Ti-2HfC	0.31785 (1)	11.2 (1)	3.78 (4)
W-3Ti-2Hf	0.317207 (7)	13.5 (1)	3.51 (3)
W-7Ti-2Hf	0.317665 (8)	12.4 (1)	3.45 (3)

Figure 1 shows the measured diffraction patterns with Rietveld refinement analysis for the sintered samples.

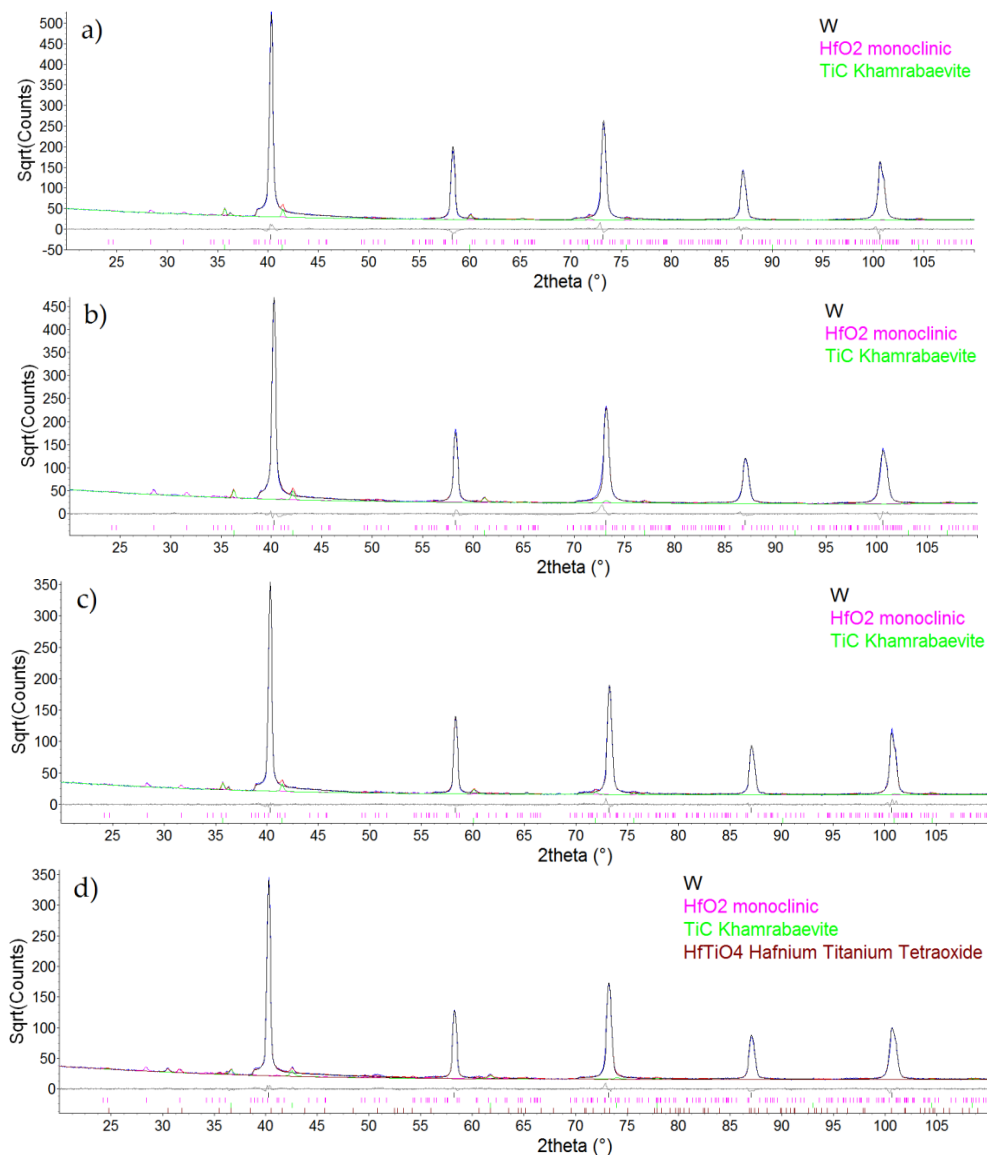


Figure 1. X-ray diffraction patterns with Rietveld refinement analysis for sintered samples, (a) W-3Ti-2HfC; (b) W-7Ti-2HfC; (c) W-3Ti-2Hf; (d) W-7Ti-2Hf.

XRD quantitative Rietveld phase analysis of sintered samples, summarized in Table 3, revealed that hafnium oxide was present in the tungsten-based matrix in the form of a monoclinic HfO_2 phase and a cubic phase with the space group $Fm\bar{3}m$. Since W, Ti and Hf all form monocarbides with

this space group and these isomorphous carbides were found miscible [10,11], a complex carbide, (Ti,W,Hf)C, was also found in all sintered samples in this work. In addition, sample W-7Ti-2Hf showed the presence of hafnium titanium tetraoxide (HfTiO₄ with the orthorhombic space group *Pbcn*). The lattice parameters of the tungsten matrix in the sintered samples (Table 4) were smaller than those of the powder samples (Table 2).

Table 3. Phase analysis of sintered samples by XRD quantitative Rietveld refinement noted in weight percent.

Identified Phases	W-3Ti-2HfC	W-7Ti-2HfC	W-3Ti-2Hf	W-7Ti-2Hf
W matrix	94.8 (6)	91.6 (4)	93.5 (8)	90.1 (8)
HfO ₂ monoclinic	0.9 (3)	2.2 (2)	1.5 (4)	2.3 (3)
(Ti,W,Hf)C	4.3 (6)	6.2 (4)	5.0 (7)	6.1 (7)
HfTiO ₄	-	-	-	1.6 (3)

Table 4. Lattice parameters of W-Ti alloy in sintered samples.

Phases	W-3Ti-2HfC	W-7Ti-2HfC	W-3Ti-2Hf	W-7Ti-2Hf
W matrix	3.16476 (7)	3.16631 (4)	3.16410 (7)	3.16464 (6)
(Ti,W,Hf)C	4.356 (1)	4.2866 (6)	4.353 (1)	4.245 (1)

The microstructure of compacted W-3Ti-2HfC and W-7Ti-2HfC shows features identical to W-3Ti-2Hf and W-7Ti-2Hf; therefore, only representative micrographs of chosen compositions will be presented here (Figure 2). Generally, the microstructure consists of regular polygonal equiaxed grains representing the W-Ti matrix and numerous smaller particles located mainly at the grain boundaries. Virtually no porosity was found in the sintered samples. According to the results of EDS (Figure 3), the brighter intergranular particles were rich in Hf and O and the darker particles were rich in Ti, an indication of Hf content being visible as well. A local increase in the C concentration was not observed due to the carbon contamination layer already present and/or deposited by the electron beam on the sample surface. Therefore, it can be expected that the lighter and darker particles are oxides (HfO₂, HfTiO₄) and a complex carbide (Ti,W,Hf)C as reported by XRD, respectively.

The size distribution of the W-Ti matrix grains is depicted in Figure 4. Local maxima within 1–5 μm² represent the most frequent area grain sizes. Lower size frequencies are not shown in the plot as they most likely represent HfO₂ particles and/or noise. The main difference between microstructures containing different amounts of Ti was that the frequency of larger carbide particles (i.e., 0.6 μm and larger) was higher for samples containing 7% Ti (Figure 5); a similar, though less obvious, trend shows the size distribution of HfO₂ (Figure 6). Fine spherical particles in the size range of tens of nanometers present within the matrix grains were more frequent in the samples containing 3% Ti (see Figure 2a).

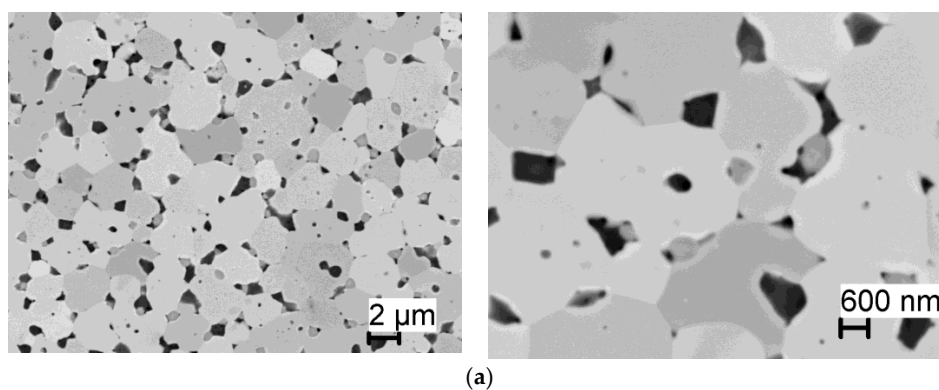


Figure 2. Cont.

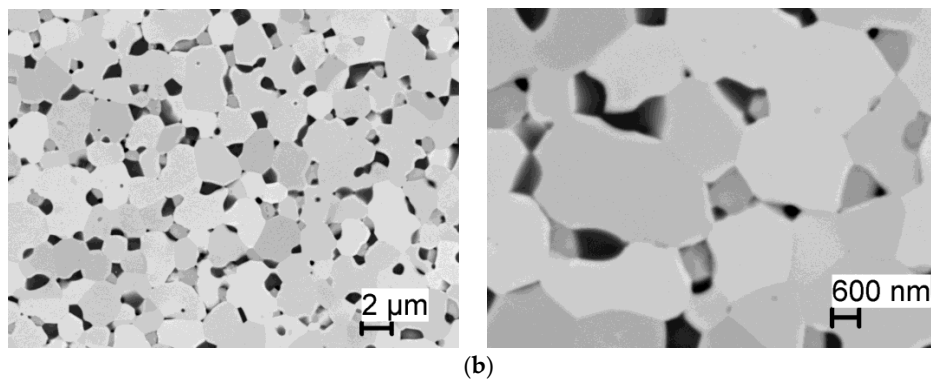


Figure 2. Microstructure of W-3Ti-2Hf and W-7Ti-2HfC consisting of W-Ti matrix (bright larger grains), (Ti,W,Hf)C (dark grains) and HfO₂ (HfTiO₄) particles (bright small grains). (a) W-3Ti-2Hf; (b) W-7Ti-2HfC.

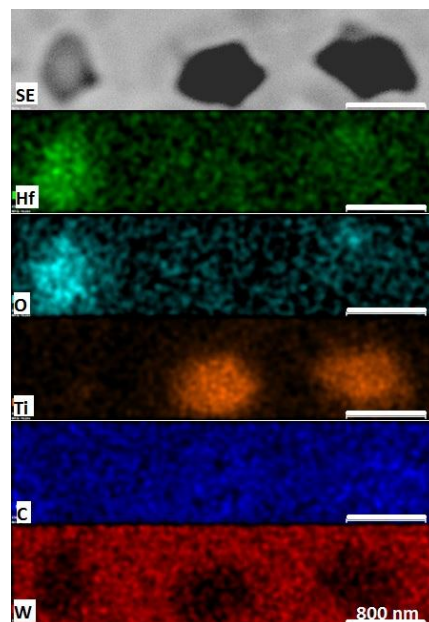


Figure 3. EDS map of area in W-3Ti-2HfC sample containing dispersed particles. All the scale bars represent the same size of 800 nm.

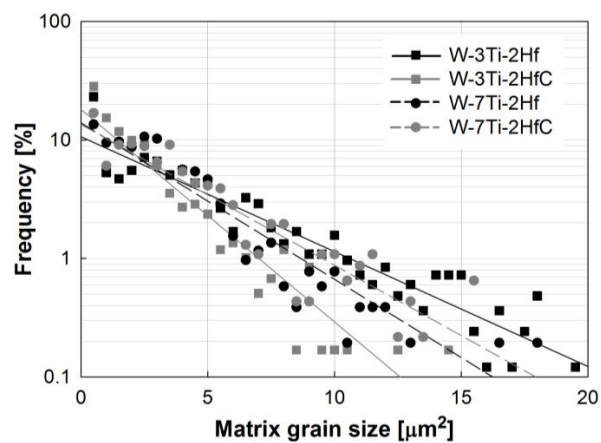


Figure 4. Frequency plot of matrix grain sizes.

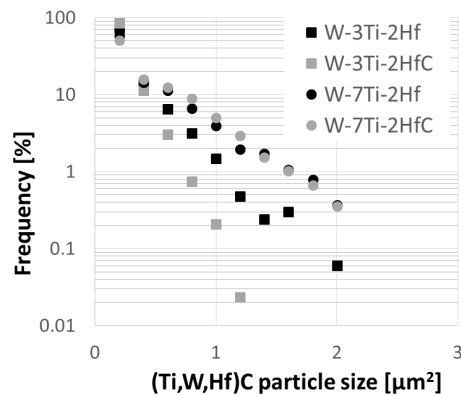


Figure 5. Frequency plot of (Ti,W,Hf)C carbide particle sizes.

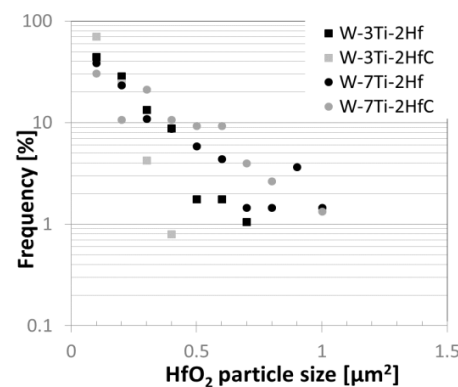


Figure 6. Frequency plot of HfO₂ (HfTiO₄) particle sizes.

3.2. Mechanical and Thermal Properties

Figure 7 summarizes results on the basic mechanical properties of the prepared alloys in comparison to pure tungsten sintered at similar conditions. A major influence of Ti content on the material strength was apparent. W-3Ti-2Hf and W-3Ti-2HfC showed an increase in the flexural strength when compared to pure tungsten whereas W-7Ti-2Hf and W-7Ti-2HfC showed a significant decrease in the strength. Slightly better values of flexural strength could be also observed for materials mechanically alloyed with the addition of HfC.

The hardness of the prepared alloys significantly increased when compared to pure tungsten. A larger increase was observed for materials containing 7% Ti. However, there was no apparent trend for the Hf/HfC content.

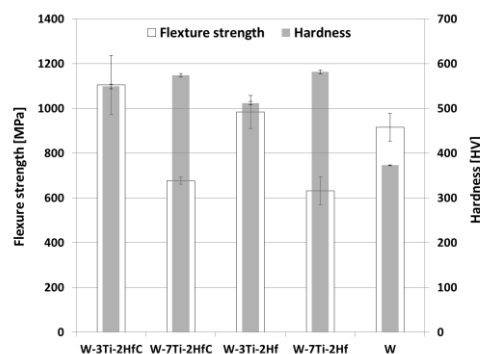


Figure 7. Flexural strength and hardness of the prepared samples in comparison with properties of pure tungsten.

The small addition of alloying elements had a significant effect on the thermal conductivity (Figure 8). In the most extreme case, i.e., for materials containing 7% Ti, the drop in the conductivity reached almost 80% at room temperature when compared to pure tungsten. The addition of HfC slightly improved the thermal conductivity at higher temperatures (above 300 °C) when compared to the materials with the addition of Hf. Generally, the thermal conductivity of metals inherently decreases with an increasing material temperature as in the case of pure tungsten. However, some alloys have an inverse dependency on the temperature, as is the case for the W-Ti-Hf(C) samples. Consequently, the difference between the prepared alloys and the pure sintered tungsten tended to decrease at higher temperatures. A minimal difference was reached for W-3Ti-2HfC above 900 °C, and for other alloys except W-7Ti-2Hf at 1300 °C. At this point, the conductivity of W-3Ti-2Hf, W-3Ti-2Hf and W-7Ti-2HfC was 20% lower than the thermal conductivity of pure tungsten.

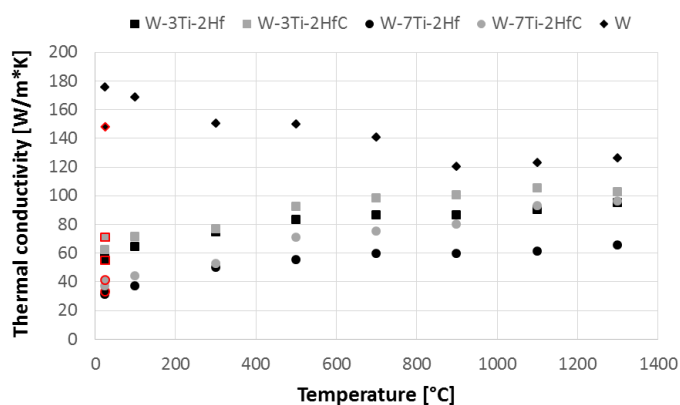


Figure 8. Thermal conductivity of the sintered samples in comparison with properties of sintered pure tungsten; points with red outlines depict the second room-temperature measurement after the high-temperature analysis.

In order to evaluate the stability of the thermal conductivity, the room-temperature value was measured twice. The first measurement was performed at 25 °C and the second measurement after the thermal cycle of the laser-flash method (appropriate points are outlined in red), i.e., after 14 h at gradually elevating temperatures from 25–1300 °C. For the W-Ti-Hf(C) samples the value of the first and second measurement is almost identical.

4. Discussion

After the sintering of the alloyed powders, new phases emerged, i.e., (Ti,W,Hf)C and HfO₂. Micrographs of the sintered materials proved the TiC phase was located at grain boundaries, where it can play an important role together with HfO₂ in grain stabilization at high temperatures by pinning grain boundaries. The dispersion of TiC particles supports the assumption of carbon surface diffusion through the powder materials and carbon grain boundary diffusion (in the later stage of sintering). The high affinity of carbon to titanium caused the depletion of excess Ti from the W-Ti matrix. Alloys with 7% Ti contained higher number of larger (Ti,W,Hf)C particles, as the higher amount of Ti led to particle coarsening. Besides the W-Ti solid solution, (Ti,W,Hf)C and HfO₂ (and HfTiO₄ in one case), the presence of additional phases was not confirmed. A number of research results reported on the formation of Ti-rich phases in W-Ti, e.g., Ti pools in W-2 wt. %Ti-0.5%Y₂O₃ and W-4 wt. %Ti-0.5%Y₂O₃ [12], in W-10 wt. %Ti [13] and in WCr₁₂Ti_{2.5} [5]. Considering the potential high-temperature applications of the alloys, the formation of Ti pools or Ti-rich solid solution is undesirable due to the low melting point of such phases (for pure titanium it is 1668 °C). The materials studied in this work maintained a high melting point, as the only Ti-rich phase confirmed by XRD was complex (Ti,W,Hf)C with a melting point most likely around that of TiC (i.e., 3160 °C), and the melting point of WC is around 2830 °C.

The matrix of the prepared materials consists of fine grains, mostly in the size range of 1 μm –5 μm diameter. It seems there is only a slight effect of the addition of titanium on the matrix grain size distribution. Alloys with 7% Ti have a slightly higher frequency of fine grains, likely due to higher occurrence of larger carbide particles.

The effect of titanium on the bending strength of the prepared materials strongly depends on the added amount of Ti. It seems there is a threshold content of titanium in W, above which the bending strength starts to decrease and becomes smaller than that of pure sintered tungsten. Nevertheless, it also seems that the effect might be different when other secondary phases are added. Authors in [14] report an opposite trend in the bending strength for W-4Ti-0.5Y₂O₃ and W-2Ti-0.47-Y₂O₃, i.e., with an increasing content of Ti, the strength increases. However, the bending strength of alloys in the mentioned study still remained below the room-temperature strength of pure tungsten. The hardness of the prepared alloys increased with respect to the pure tungsten due to the increase in the dislocation density caused by ball milling, grain refinement and mainly due to the presence of hard particle dispersion. The hardness value was slightly lower for alloys containing 3% Ti as the frequency of carbide particles in each size category was lower.

The results of the thermal conductivity showed a major decrease for the prepared alloys when compared to pure tungsten. According to the rule of mixture and the Maxwell-Garnett model applied on W-3Ti-2HfC and W-7Ti-2HfC with respect to the volumetric representation of the XRD results, the room-temperature thermal conductivity due to the second-phase dispersion should not decrease by more than 26% (according to rule of mixture the values are 155 W/(K·m) and 144 W/(K·m), respectively; according to the Maxwell-Garnett model they are 146 W/(K·m) and 133 W/(K·m), respectively) [15]. The calculated numbers were significantly higher than the measured values which might imply a significant influence of Ti dissolved in the tungsten lattice. The thermal conductivity of the prepared materials grew with the temperature, which is a less common phenomenon. That can also be attributed to the Ti dissolved in the W matrix. However, from 900 °C the thermal conductivity of W-3Ti-HfC alloy was only 20 W/(K·m) smaller than that of pure tungsten. Although at higher temperatures the difference in the thermal conductivity was minimized, the authors believe that an additional improvement might be possible by lowering the titanium content or additional thermomechanical processing. For example, in [16] a dramatic improvement of thermal conductivity for W-TaC alloys was reached after hot rolling.

The lower rate in the thermal conductivity increase for W-7Ti-2Hf was probably caused by the presence of HfTiO₄.

5. Conclusions

Four types of tungsten materials were prepared in this study, i.e., W-3Ti-2Hf, W-3Ti-2HfC, W-7Ti-2Hf and W-7Ti-2HfC. Due to the sintering in the presence of graphite, a certain amount of Ti and Hf was transformed into the complex carbide phase. Thus, no Ti pools were formed, unlike in the results in a number of other studies. The microstructure consisted of a W-Ti matrix with fine (Ti,W,Hf)C and HfO₂ particles dispersed at the grain boundaries. Besides the mixed Hf-Ti oxide in the sample with the highest Ti content, no other phases within a detectable limit were present. It can thus be expected that the prepared alloys possess a high melting point and can be applied in high-temperature environments. Moreover, it can be expected that the particle dispersion improves the high-temperature stability.

The effect of the addition of titanium on the materials' strength was found to depend on the amount of Ti added. The bending strength of the alloys with 3% Ti increased with respect to pure tungsten, whereas 7% Ti led to a significant decrease in strength.

The addition of Ti into tungsten significantly lowers the thermal conductivity which is the major drawback of the prepared alloys. Nevertheless, it was proved that the conductivity has a tendency to increase with the temperature. Thus, in the temperature window predicted for future fusion

reactors, i.e., between 700 °C and 1300 °C, the conductivity reached nearly the value of conductivity for pure tungsten.

Acknowledgments: This work was financially supported by the grant GAČR 15-15609S. One author, O.M., is grateful for financial support from the grant SVV-2016-260213.

Author Contributions: All the authors contributed equally to this research by conducting the experiments and by finalization of the manuscript. F.L., M.V. and T.C. contributed with preparation and finalization of manuscript, F.L. with XRD method results, M.V. with SEM method results, milling and sintering optimization, B.N. with laser-flash method, J.K. with mechanical properties testing, O.M. with powders and samples preparation.

Conflicts of Interest: The authors declare no conflict of interest.

References

1. Shu, W.M.; Kawasuso, A.; Yamanishi, T. Recent findings on blistering and deuterium retention in tungsten exposed to high-fluence deuterium plasma. *J. Nucl. Mater.* **2009**, *386–388*, 356–359. [[CrossRef](#)]
2. El-Atwani, O.; Gonderman, S.; Efe, M.; de Temmerman, G.; Morgan, T.; Bystrov, K.; Klenosky, D.; Qiu, T.; Allain, J.P. Ultrafine tungsten as a plasma-facing component in fusion devices: Effect of high flux, high fluence low energy helium irradiation. *Nucl. Fusion* **2014**, *54*, 83013. [[CrossRef](#)]
3. Rieth, M.; Boutard, J.L.; Dudarev, S.L.; Ahlgren, T.; Antusch, S.; Baluc, N.; Barthe, M.-F.; Becquart, C.S.; Ciupinski, L.; Correia, J.B.; et al. Review on the EFDA programme on tungsten materials technology and science. *J. Nucl. Mater.* **2011**, *417*, 463–467. [[CrossRef](#)]
4. Vilémová, M.; Pala, Z.; Jäger, A.; Matějček, J.; Chernyshova, M.; Kowalska-Strzęciwilk, E.; Tonarová, D.; Gribkov, V.A. Evaluation of surface, microstructure and phase modifications on various tungsten grades induced by pulsed plasma loading. *Phys. Scr.* **2016**, *91*, 34003. [[CrossRef](#)]
5. López-Ruiz, P.; Ordás, N.; Iturriza, I.; Walter, M.; Gaganidze, E.; Lindig, S.; Koch, F.; García-Rosales, C. Powder metallurgical processing of self-passivating tungsten alloys for fusion first wall application. *J. Nucl. Mater.* **2013**, *442*, S219–S224. [[CrossRef](#)]
6. Rietveld, H.M. Line profiles of neutron powder-diffraction peaks for structure refinement. *Acta Crystallogr.* **1967**, *22*, 151–152. [[CrossRef](#)]
7. Coelho, A.A. *TOPAS*, version 5 (Computer Software); Coelho Software: Brisbane, Australia, 2016.
8. Waseda, Y.; Hirata, K.; Ohtani, M. High-temperature thermal expansion of platinum, tantalum, molybdenum, and tungsten measured by X-ray diffraction. *High Temp. High Press.* **1975**, *7*, 221–226.
9. Lvinger, W.B. Lattice parameters of beta titanium at room temperature. *J. Met.* **1953**, *5*, 195.
10. Rudy, E. Constitution of ternary titanium-tungsten-carbon alloys. *J. Less Common Met.* **1973**, *33*, 245–273. [[CrossRef](#)]
11. Murray, P.; Weston, J.E. The 1700 °C isothermal section of the pseudoternary system TiC-ZrC-HfC. *J. Less Common Met.* **1981**, *81*, 173–179. [[CrossRef](#)]
12. Aguirre, M.V.; Martín, A.; Pastor, J.Y.; LLorca, J.; Monge, M.A.; Pareja, R. Mechanical properties of Y₂O₃-doped W-Ti alloys. *J. Nucl. Mater.* **2010**, *404*, 203–209. [[CrossRef](#)]
13. Dai, W.; Liang, S.; Luo, Y.; Yang, Q. Effect of W powders characteristics on the Ti-rich phase and properties of W-10 wt. % Ti alloy. *Int. J. Refract. Met. Hard Mater.* **2015**, *50*, 240–246. [[CrossRef](#)]
14. Aguirre, M.V.; Martín, A.; Pastor, J.Y.; LLorca, J.; Monge, M.A.; Pareja, R. Mechanical properties of tungsten alloys with Y₂O₃ and titanium additions. *J. Nucl. Mater.* **2011**, *417*, 516–519. [[CrossRef](#)]
15. Garnett, J.C.M. Colours in Metal Glasses, in Metallic Films, and in Metallic Solutions. II. *Philos. Trans. R. Soc. Math. Phys. Eng. Sci.* **1906**, *205*, 237–288. [[CrossRef](#)]
16. Miao, S.; Xie, Z.M.; Yang, X.D.; Liu, R.; Gao, R.; Zhang, T.; Wang, X.P.; Fang, Q.F.; Liu, C.S.; Luo, G.N.; et al. Effect of hot rolling and annealing on the mechanical properties and thermal conductivity of W-0.5 wt. % TaC alloys. *Int. J. Refract. Met. Hard Mater.* **2016**, *56*, 8–17. [[CrossRef](#)]

